Soft-x-ray fluorescence study of the quasi-one-dimensional Heisenberg antiferromagnet tetraphenylverdazyl

E. Z. Kurmaev and V. R. Galakhov
Institute of Metal Physics, Russian Academy of Sciences-Ural Division, 620219 Yekaterinburg GSP-170, Russia

S. Shimada, T. Otsuka, and K. Endo
Department of Chemistry, Faculty of Science, Kanazawa University, Kakuma-machi, Kanazawa, 920-1192 Japan

S. Stadler
Materials Physics Division, Naval Research Laboratory, Washington, D.C. 20375

D. L. Ederer
Department of Physics, Tulane University, New Orleans, Louisiana 70118

A. Moewes
CAMD, Louisiana State University, 6980 Jefferson Highway, Baton Rouge, Louisiana 70806

H. Schuerman and M. Neumann
Universitat Osnabrück, Fachbereich Physik, D-49069 Osnabrück, Germany

S. Tomiyoshi and N. Azuma
Department of Materials Science and Engineering and Department of Chemistry, Ehime University, Matsyama 790, Japan

M. Iwami
Research Laboratory for Surface Science, Okayama University, Okayama 700-8530, Japan
(Received 6 April 2000; revised manuscript received 31 July 2000)

Soft-x-ray fluorescence measurements have been performed on a single crystal of the organic antiferromagnet 2,4,6-triphenylverdazyl. Resonant and nonresonant C $K\alpha$ and N $K\alpha$ ($2p \rightarrow 1s$ transition) x-ray emission spectra (XES) were measured and compared with x-ray photoelectron valence band spectra and deMon density-functional theory calculations. It is shown that intramolecular interactions are much stronger than intermolecular ones and give the main contribution to the formation of C $2p$ density of states. We present evidence of a delocalization of unpaired N $2p$ electrons over the verdazyl ring. The excitation energy dependence of C $K\alpha$ and N $K\alpha$ XES observed below the C $1s$ and N $1s$ thresholds, respectively, is discussed in terms of symmetry selective resonant inelastic x-ray scattering.

I. INTRODUCTION

The class of stable free radicals called the verdazyls synthesized by Kuhn and Trischmann[1] is of great interest because of their unusual magnetic properties. 2,4,6-triphenylverdazyl (TPV) shows an antiferromagnetic ordering with a Néel temperature of 1.7 K accompanied by a weak ferromagnetic component,[2–4] whereas, 2,4,6-tri-*p*-tolylverdazyl (TTV) is paramagnetic.[5] According to Ref. 5, the different molecular packing, which leads to changes in overlapping of orbitals occupied by unpaired $2p$ electrons, can cause different magnitudes of exchange interaction. In connection with this, a detailed study of the electronic structure of the organic antiferromagnet TPV is very important.

In this paper, we present the results of soft-x-ray fluorescence measurements of a TPV single crystal. The resonant and nonresonant C $K\alpha$ and N $K\alpha$ ($2p \rightarrow 1s$ transition) x-ray emission spectra (XES) were measured at Beamline 8.0 of the Advanced Light Source (LBNL, Berkeley), and compared with the x-ray photoelectron valence-band spectrum (XPS VB) and deMon density-functional theory (DFT) calculations. Evidence for a delocalization of unpaired N $2p$ electrons over the verdazyl ring is found, which is in accordance with the spin-density distribution of TPV. We show that intermolecular interactions are weaker than the intramolecular ones, which allows us to conclude that the electronic structure of TPV crystal has a quasi-one-dimensional character. We also discuss the excitation energy dependence of C $K\alpha$ and N $K\alpha$ emission spectra observed for near-threshold excitation with respect to the symmetry-selective resonant inelastic x-ray scattering.

II. EXPERIMENTAL AND CALCULATION DETAILS

A polycrystalline sample of TPV was prepared in a similar manner to that of Kuhn and Trischmann,[1] and comparatively large single-crystal samples were grown by using recrystallization from an acetone solution. The crystals thus obtained have a hexagonal plate with its plane normal to the *a* axis and its long edge along the *c* axis.

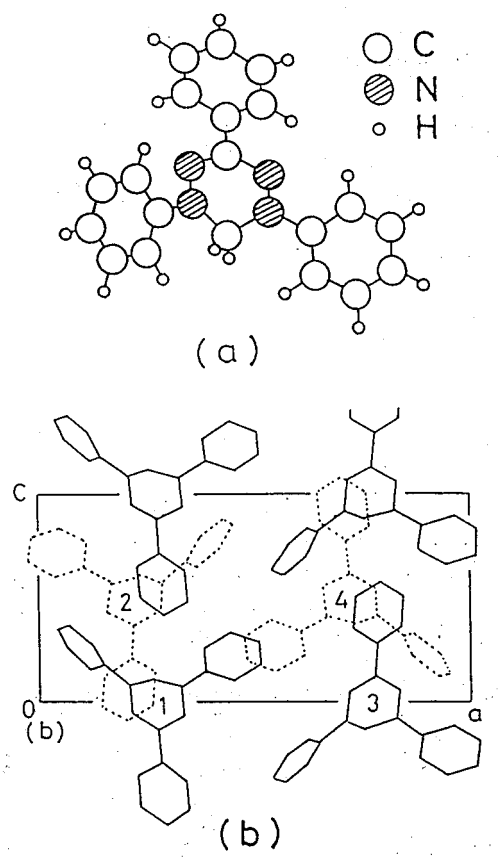

FIG. 1. Molecular structure of TPV (a) and crystal structure of TPV projected on the a-c plane (b).

Carbon and nitrogen $K\alpha$ ($2p \rightarrow 1s$ transition) XES were taken at Advanced Light Source (Beamline 8.0), employing the University of Tennessee at Knoxville's soft-x-ray fluorescence endstation.[6] Photons with energies of 280–298 eV, near the carbon K edge and with energies of 393–404 eV, near the nitrogen K edge were delivered to the endstation via the beamline's spherical grating monochromator. The carbon and nitrogen $K\alpha$ spectra were obtained with an energy resolution of 0.5 and 1 eV, respectively. The photon flux was continuously monitored using a gold mesh in front of the sample and the measurements were normalized with respect to this current.

The XPS measurements have been carried out with a PHI 5600 ci-type ESCA spectrometer using monochromatized Al $K\alpha$ radiation with 0.3 eV full width at half maximum (FWHM). The energy resolution of the analyzer was 1.5% of the pass energy. We estimate the energy resolution of the spectrometer to be better than 0.35 eV. The pressure in the vacuum chamber during the measurements was below 5×10^{-9} mbar. The TPV crystal was cleaved in an ultrahigh vacuum for XPS measurements in order to obtain spectra from a surface free of contaminants. All measurements were performed at room temperature. The XPS spectra were calibrated using the Au $4f_{7/2}$ signal from Au foil whose binding energy is 84.0 eV.

The calculation of TPV is not trivial due to the rather complicated molecular and crystal structure. The molecular structure of TPV [see Fig. 1(a)] consists of a verdazyl ring in the center surrounded by three phenyl groups with hydrogen side groups.[5] TPV molecules are arranged in zigzag chains along the c axes [Fig. 1(b)]. TPV crystallizes in the orthorhombic structure with four molecules per unit cell,[7] which makes first-principles band-structure calculations extremely difficult. We have performed deMon DFT calculations for one molecule, neglecting interchain interactions.

The geometry of the radical compound 2,4,6-TPV was optimized in the self-consistent-field calculation of unrestricted Hartree-Fock equations by semiempirical molecular orbital (MO) AMI method in MOPAC software.[8] The molecule includes a total amount of 41 atoms including 20 carbon atoms, 4 nitrogen atoms, and 17 hydrogen atoms [with a total of 165 electrons, total of 117 orbitals and (59 and 58) occupied α and β orbitals, respectively]. The calculation shows that the π-positive spin density is mostly localized as [(0.10, 0.46) and (0.21, 0.36)] on the (p_y, p_z) orbitals of two $N_1{=}N_2$ bonding nitrogens in the verdazyl ring, respectively, and the negative- and positive-spin densities are polarized alternately through bonds on the p_y and p_z orbitals of carbons for the verdazyl and three phenyl rings. The spin-density distribution agrees well with the results calculated by Azuma.[5]

The intensity of the spectral line is given by

$$\tau_{if} \propto \left| \int \Phi_i P \Phi_f d\tau \right|^2, \tag{1}$$

where P, Φ_i, and Φ_f are the associated transition operator, the initial, and excited final states, respectively. In the case of the valence XPS, the intensity is related to the photoionization cross section of the molecular orbitals. For the x-ray emission spectra, the transitions are governed by selection rules, meaning that the orbital angular momentum-quantum number is constrained to change according to the relation $\Delta l = \pm 1$. For example, the observed electron transitions in the carbon atoms of the TPV films arise from the filling of s-type ($l=0$) holes by occupied orbitals with a p character ($l=1$) in the same atom. We can obtain the calculated values for the XES emission energies from the differences between binding energies of the core level where the hole is created and vertical ionization potentials (VIP's) of the electrons that fill the core hole.

In order to simulate the valence XPS and XES, we used the deMon DFT program.[9] The deMon calculations were performed using B88/P86 exchange-correlation potential obtained from Becke's 1988 exchange functional[10] and Perdew's 1986 correlation functional.[11] The intensity of carbon and nitrogen $K\alpha$ XES was obtained by summing populations [squares of the linear combination of atomic orbitals coefficients] of the atomic orbitals $\chi_{2p(A)}(r)$ centered on the given nitrogen or carbon atoms. We approximated the populations as obtained from the deMon DFT calculations of the TPV molecule with Slater-type orbitals (STO)-$3G$ basis set. Each peak in the theoretical XES spectra is also represented by a Gaussian line-shape function, with the same weight and full width at half-maximum FWHM=1.3 eV as the experimental spectra. For the simulation of the valence XPS, we used the Gaussian functions of line width of the peaks proportional to the ionization energy, implying that the spectra of the inner valence levels are broader, to incorporate the lifetime broadening.[12] The calculated spectra showed a good agree-

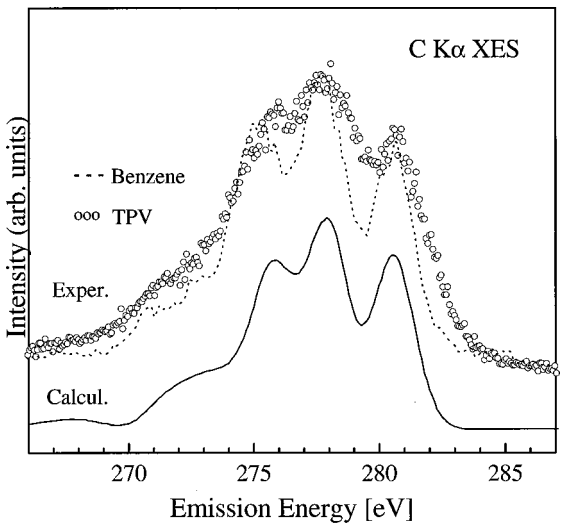

FIG. 2. Nonresonant C $K\alpha$ XES of TPV and benzene (Ref. 9) and calculated C $K\alpha$ emission spectrum.

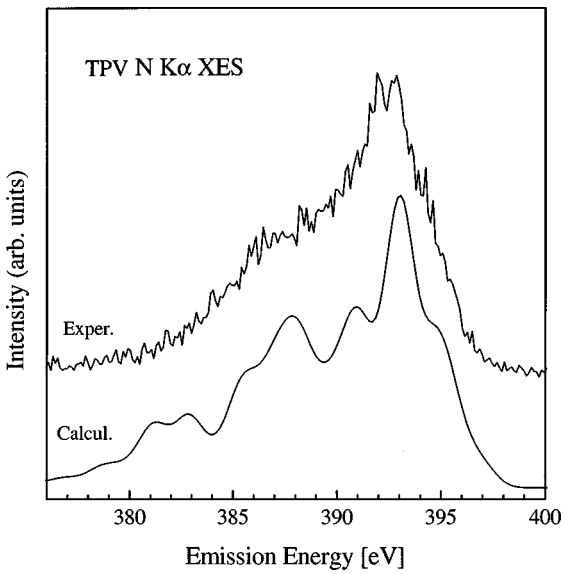

FIG. 3. Nonresonant N $K\alpha$ emission spectrum and calculated N $K\alpha$ emission of TPV.

ment with the experiment, allowing a detailed analysis of occupied molecular orbitals of TPV.

III. RESULTS AND DISCUSSION

A. Nonresonant x-ray emission spectra

The nonresonant x-ray emission spectra are measured by exciting above the core-ionization threshold. In this case, the fine structure of x-ray emission is practically independent of the excitation energy. The spectral shape of x-ray emission can be described with the emission decoupled from the excitation. The first step corresponds to an electron transition from a core level to an empty valence level when the sample absorbs an incident photon. The second step is the emission of a photon when an electron undergoes a transition from an occupied valence level to fill the core hole created by the incident photon absorption. Both steps are governed by the dipole selection rule, $\Delta l = \pm 1$, which means that the $1s$ core level holes in carbon and nitrogen can only be filled by $2p$ valence electrons. Therefore, in nonresonant x-ray emission spectra of light elements, the intensities map the p density at each particular atomic site, and in a MO picture, the contribution of the local p-type atomic orbitals.

The nonresonant carbon $K\alpha$ XES of TPV excited at $E_{\mathrm{exc}} = 298.7$ eV is shown in Fig. 2. The spectrum of benzene[13] is also included for comparison. The fine structure of C $K\alpha$ XES of TPV resembles that of benzene because the chemical structure of TPV consists of three phenyl groups. The calculated C $K\alpha$ spectrum reproduces the experimental one of TPV quite well. Table I displays the positions of observed C $K\alpha$ peaks, the calculated emission energies, the orbital nature, and the functional groups of the TPV films. Good agreement between the experimental C $K\alpha$ spectrum of the TPV crystal and the calculated C $K\alpha$ spectrum of a model molecule shows that the intermolecular interactions are smaller than the intramolecular ones. This is not contradictionary to quasi-one-dimensional electronic and magnetic properties for this compound found by electron spin resonance (ESR) measurements of TPV.[4] According to these measurements, ESR line shape and line width are typical for a one-dimensional Heisenberg antiferromagnet. The nonresonant N $K\alpha$ XES of TPV excited at around 400 eV is presented in Fig. 3 together with the calculated spectrum. Table II shows the positions of observed N $K\alpha$ peaks, the calculated emission energies, the orbital nature, and the func-

TABLE I. Observed peaks, emission energy, orbital nature, and functional group (FG) for nonresonant C $K\alpha$ XES of TPV.

Observed peak (eV)	Emission energy [(CEBE)−(VIP)] (eV)	Orbital nature	FG
272.0	272.3	p_σ (C $2p$–C $2s$)–B	-C-C
(270–274)		p_π (C $2p$–N $2p$)–B	-C-N
276.0	276.1	p_π (C $2p$–C $2p$)–B	-C-C
(275.5–276.5)			
277.8	277.8	p_π (C $2p$–C $2p$)–B	-C-C
(277–278.5)			
280.7	280.5	p_π (C $2p$–N $2p$)–B	-C-N
(280–282)			

TABLE II. Observed peaks, emission energy, orbital nature, and functional group for nonresonant N $K\alpha$ XES of TPV.

Observed peak (eV)	Emission energy [(CEBE)−(VIP)] (eV)	Orbital nature	FG
382.0	381.0	p_σ(N 2p–C 2s)–B	-N-N
(380.5–384)	382.6	p_σ(N 2p–N 2s)–B	-N-C
		p_π(N 2p–N 2p)–B	
385.8, 386.8	386.3	p_π(N 2p–N 2p)–B	-N-N
(385–389)	387.7	p_π(N 2p–C 2p)–B	-N-C
390.2	391.2	p_π(N 2p–N 2p)–B	-N-N
(390–392)		p_π(N 2p–C 2p)–B	-N-C
393.5	393.3	p_π (lone pair)–NB	-N
(392–394)		p_z (odd electron)	-N
shoulder	395.2	P_z (odd electron)	-N
(394–395.5)			

tional groups of the TPV films. We note that the spectral shapes of the experimental and calculated spectra are very similar. According to the calculation, unpaired N 2p electrons are delocalized over the verdazyl ring, which was predicted in Ref. 3 based on the analysis of the magnetic properties of TPV. Azuma *et al.*[3] pointed out that the spin density is distributed over four nitrogen atoms in the verdazyl ring, which implies the delocalization of the unpaired electron over the TPV molecule.

Therefore, a good agreement between experimental and calculated nonresonant N $K\alpha$ XES of TPV means that we have evidence of the delocalization of unpaired electrons over the TPV molecule, which is considered the most characteristic feature of the magnetism of TPV.[2]

B. Resonant x-ray emission spectra

By using tunable synchrotron radiation, the excitation energy is tuned through the photoabsorption threshold. The observed x-ray emission spectra can be strongly dependent on the excitation energy due to differently populated intermediate states. In the theoretical description, excitation and relaxation are no longer independent[14] and are treated as one scattering event. The proposed explanation for the XES intensity variations for solids (for instance, for diamond[15] and graphite[16]) is based on considering the x-ray fluorescence as a scattering process, in which momenta of the photoelectron and the valence hole in the final state are related by momentum conservation. In the resonant x-ray emission of molecules, the parity should be conserved in the full absorption-emission scattering process.[17] This means that if a core electron is promoted to an orbital of gerade (ungerade) symmetry only electrons from gerade (ungerade) orbitals are allowed to fill the core hole. As a result, some spectra features seen in nonresonant spectra should be depleted in the resonance regime due to the symmetry selection.

The C $K\alpha$ and N $K\alpha$ emission of TPV, excited at various photon energies near the threshold, are displayed in Figs. 4 and 5. The resonant XES spectrum consists of the inelastic scattering contribution and the elastic (recombination) peak with an energy position equivalent to the excitation energy. The inelastic scattering contribution to C $K\alpha$ XES of TPV shows a dependence on the excitation energy, especially below the ionization thresholds. In the absence of measurements of x-ray absorption spectra, we can roughly estimate the C 1s and N 1s ionization thresholds from XPS core level binding energies [$E_{\text{b.e.}}$(C 1s) = 286.0 eV and $E_{\text{b.e.}}$(N 1s) = 400.5 eV].

The resonant C $K\alpha$ XES of TPV (Fig. 4) show a three-peak structure (*a, b, c*) for all excitation energies. However, the intensities of peaks *a* and *b* are decreased in the spectra measured below the 1s threshold (at E_{exc} = 283.9–285.8 eV). In spite of some similarity with the nonresonant spectra (Fig. 2), the resonant C $K\alpha$ XES of TPV (Fig. 4) and benzene[13] are found to be different. In the resonant spectra of benzene (see Fig. 4) the intensity in the energy range 280–284 eV is fully absent due to strict parity selection rules.[13] However, by lowering the symmetry from D_{6h} (benzene) to C_1 (TPV), the parity selection rule no longer holds. Therefore, one could expect that the resonant

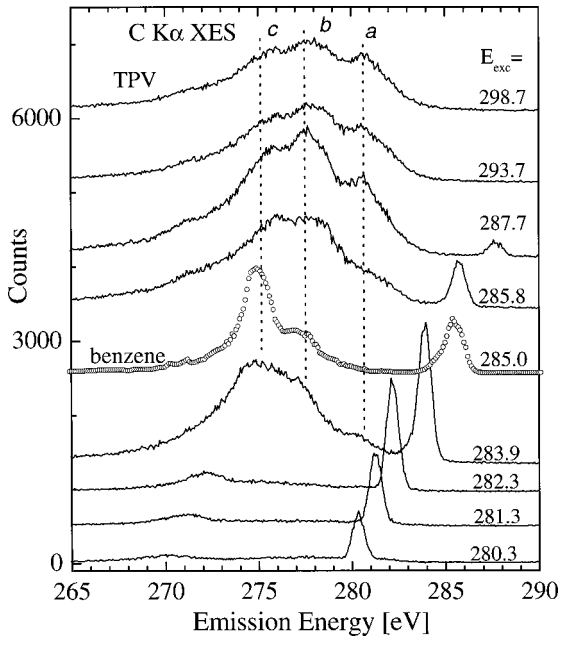

FIG. 4. Excitation energy dependent C $K\alpha$ XES of TPV.

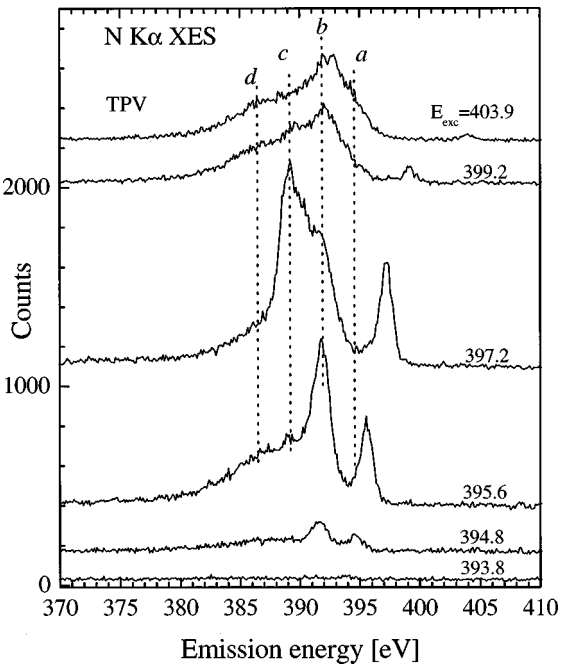

FIG. 5. Excitation energy dependent N $K\alpha$ XES of TPV.

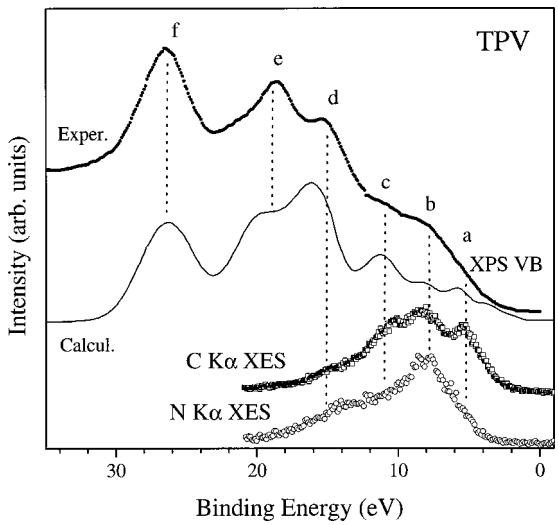

FIG. 6. Experimental and calculated photoelectron valence band spectra (XPS VB) and their comparison with nonresonant C $K\alpha$ and N$K\alpha$ of TPV.

and nonresonant C $K\alpha$ XES of TPV would be similar. The experimental C $K\alpha$ spectra for TPV therefore, show benzenelike features also in the case of resonant excitation with the band *a* intensity considerably reduced. According to Fig. 1, carbon atoms occupy three nonequivalent positions in the TPV crystal structure. Our XPS measurements show that the C 1*s* line is broad, which can be due to the superposition of three lines with subelectron-volt chemical shifts. Therefore, we suggest that the superposition of different close-lying 1*s* core hole states in resonantly excited C $K\alpha$ emission spectra leads to the decrease in the signal.[18]

More noticeable changes are found in the resonantly excited N $K\alpha$ XES of TPV (Fig. 5): only peaks *b* and *c* are observed below the threshold, whereas peaks *a* and *d* are depleted or have low intensity. There are two nonequivalent nitrogen atoms in the structure of TPV (Fig. 1) that give raise to a broad XPS N 1*s* line and therefore the depletion of peaks *a* and *d* under resonant excitation of N *K*a XES can be attributed to interference effects as well.[19,20]

C. X-ray photoelectron valence-band spectrum

The results of the XPS VB measurements of TPV are shown in Fig. 6. The XPS VB of TPV consists of six overlapping subbands labeled *a* through *f*. For analysis of the experimental spectrum, DFT calculations of the model monomer $(H_3CC_6H_4)N[C_6H_4(CH{=}CH_2)]_2$ were performed using the deMon program. The results of the deMon DFT calculations of the XPS VB of TPV are shown in Fig. 6 and Table III. Table III displays the positions of observed XPS VB peaks, the calculated VIP's the main atomic orbitals, the orbital nature, and the functional groups of the TPV films. The calculated XPS VB spectrum (for a model molecule) shows a very good correspondence with the experimental one (see Fig. 6). Energy positions and intensities of the observed peaks are reproduced quite well, which supports the conclusion that intermolecular interactions in the TPV crystal are very weak.

The most intense experimental peak *f*, located around 26.0 eV, corresponds to the ionization of $[s_\sigma(\mathrm{N}\,2s{-}\mathrm{N}\,2s, \mathrm{C}\,2s){-}\mathrm{B}]$ bonding orbitals, resulting from the N-N and C-N functional groups of TPV. Peak *e*, located at $\sim$ 18.7 eV, can be attributed to contributions from $[\{s_\sigma(\mathrm{C}\,2s{-}\mathrm{C}\,2s), s_\sigma(\mathrm{C}\,2s{-}\mathrm{C}\,2s),\mathrm{N}\,2s\}{-}\mathrm{B}]$ bonding orbitals from C-C and C-C, C-N functional groups, respectively. Peak *d* around 15.2 eV is related to contributions from $s_\sigma(\mathrm{C}\,2s{-}\mathrm{C}\,2s){-}\mathrm{B}$ and $s_\sigma(\mathrm{C}\,2s{-}\mathrm{C}\,2s){-}\mathrm{B}$ bonding orbitals from C-C and C-C functional groups. The next peak labeled *c* around 11.0 eV is due to contributions from $p_\sigma(\mathrm{C}\,2s{-}\mathrm{N}\,2p){-}\mathrm{B}$, $p_\sigma(\mathrm{C}\,2s{-}\mathrm{C}\,2p){-}\mathrm{B}$, $p_\sigma,p_\pi(\mathrm{C}\,2p{-}\mathrm{C}\,2p,\mathrm{N}\,2p){-}\mathrm{B}$, and $p_\sigma(\mathrm{C}\,2p{-}\mathrm{C}\,2p){-}\mathrm{B}$ bonding orbitals from C-N, C-C, C═C/C═N, and C═C functional groups, respectively. The broad peak *b* at $\sim$ 8.0 eV is generated by contributions from $p_\pi(\mathrm{C}\,2p{-}\mathrm{C}\,2p,\mathrm{N}\,2p){-}\mathrm{B}$ bonding orbitals from C═C and C═N groups, respectively. Finally, we attribute peak *a* located around 5.1 eV to $p_\pi(\mathrm{C}\,2p{-}\mathrm{C}\,2p,\mathrm{N}\,2p)$ bonding orbitals from C═C and C═N functional groups and $p_\pi\mathrm{N}\,2p$ lone-pair nonbonding orbitals.

However, it is rather difficult to determine the orbital composition of the occupied molecular orbitals and to verify the DFT calculations of TPV-TTV by only using XPS measurements that provide information about the total density of states. In this respect, the measurements of x-ray emission spectra are very useful because they directly probe the partial density of states of the constituent atoms in compounds due to the dipole selection rules. We have compared XPS VB and nonresonant C $K\alpha$ and N $K\alpha$ XES of TPV in the binding energy scale in Fig. 6. The experimental XES spectra are converted to the binding energy scale using our XPS measurements of the core levels. The subbands *d* through *f* are practically not observed in C $K\alpha$ and N $K\alpha$ XES of TPV because $2s\rightarrow1s$ transitions are forbidden by dipole selection rules. On the other hand, the upper $a{-}c$ subbands of XPS VB are very close in energy with C $K\alpha$ and N $K\alpha$ XES, which also exhibit the three-peak fine structure. Therefore, we have an evidence of strong mixing of C 2*p* and N 2*p* valence states, which is in accordance with results of deMon

TABLE III. Observed peaks, vertical ionization potential (VIP), main photoelectron ionization cross-section of the atomic orbitals (AO PICS), orbital nature, and the functional group (FG) for XPS VB of TPV (charge +1). (The difference between observed and calculated VIP's is 8.9 eV).

Peak (eV)	VIP (eV)	Main AO PICS	Orbital nature	FG
26.0	27.4, 26.0	C 2*s* (0.1), N 2*s* (0.9)	s_σ (N 2*s*–N 2*s*, C 2*s*)–B	N-N, C-N
	21.6	C 2*s* (0.6), N 2*s* (0.4)	s_σ (N 2*s*–N 2*s*, C 2*s*)–B	N-N, C-N
18.7	20.4–19.2	C 2*s* (0.8), N 2*s* (0.2)	s_σ (C 2*s*–C 2*s*)–B	C-C
	17.9, 17.4	C 2*s* (0.6), N 2*s* (0.3)	s_σ (C 2*s*–C 2*s*, N 2*s*)–B	C-C, C-N
15.2	16.6–16.4	C 2*s*	s_σ (C 2*s*–C 2*s*)–B	C-C
	15.7–14.9	C 2*s* (0.7), N 2*s* (0.3)	s_σ (C 2*s*–C 2*s*)–B	C-C
11.1	12.9–10.1	C 2*s*, N 2*s*, N 2*p*	p_σ (C 2*s*–N 2*p*)–B	C-N
	9.5–8.1	C 2*s*, N 2*s*, N 2*p*	p_σ (C 2*s*–C 2*p*)–B	C-C
			$p_\sigma p_\pi$ (C 2*p*–C 2*p*, N 2*p*)–B	C═C, C═N
			p_σ (C 2*p*–C 2*p*)–B	C═C
8.0	7.9–7.1	C 2*p*, N 2*p*	p_π (C 2*p*–C 2*p*, N 2*p*)–B	C═C, C═N
5.1	6.8–5.0	C 2*p*, N 2*p*	p_π (C 2*p*–C 2*p*, N 2*p*)–B	C═C, C═N
	4.2–2.1	N 2*p*	p_π (lone pair)–NB	-N-

DFT calculations. Good agreement between experimental and calculated XPS VB spectra shows that the model molecule used in our deMon DFT calculations provides a good description of spectral properties of TPV molecular crystal.

IV. CONCLUSION

In summary, we have studied the electronic structure of the quasi-one-dimensional Heisenberg antiferromagnet triphenylverdazyl by means of x-ray emission and photoelectron spectroscopy, and compared our experimental data with deMon DFT calculations. The orbital composition of occupied molecular orbitals is determined. We have found evidence for a delocalization of unpaired N 2*p* electrons over the verdazyl ring, which is also supported by results from the analysis of the magnetic properties of this compound. It is shown that intramolecular interactions are much stronger than intermolecular ones and give the main contribution to the formation of C 2*p* density of states. Strong intensity modulations of spectral features are found in C $K\alpha$ and N $K\alpha$ XES of TPV with varying excitation energy near the C 1*s* and N 1*s* thresholds, which is analyzed in terms of symmetry-selective resonant scattering process.

ACKNOWLEDGMENTS

This work was supported by the Russian Science Foundation for Fundamental Research (Project Nos. 00-15-96575 and 99-03-32503), NSF Grant Nos. DMR-901 7997 and DMR-9420425, and the DOE EPSCOR and Louisiana Education Quality Special Fund [DOE-LEQSF (1993-95-03)].

[1] R. Kuhn and H. Trischmann, Angew. Chem. **75**, 294 (1963); R. Kuhn and H. Trischmann, Monatsch. Chem. **95**, 457 (1964).
[2] S. Tomiyoshi, T. Yano, N. Azuma, M. Shoga, K. Yamada, and J. Yamauchi, Phys. Rev. B **49**, 16 031 (1994).
[3] N. Azuma, J. Yamauchi, K. Mukai, H. Ohya-Nishiguchi, and Y. Deguchi, Bull. Chem. Soc. Jpn. **46**, 2728 (1973).
[4] B. Pilawa, J. Magn. Magn. Mater. **140-144**, 1653 (1995).
[5] N. Azuma, Bull. Chem. Soc. Jpn. **55**, 1357 (1982).
[6] J. J. Jia, T. A. Callcott, J. Yurkas, A. W. Ellis, F. J. Himpsel, M. G. Samant, J. Stöhr, D. L. Ederer, J. A. Carlisle, E. A. Hudson, L. J. Terminello, D. K. Shuh, and R. C. C. Perera, Rev. Sci. Instrum. **66**, 1394 (1995).
[7] D. E. Williams, Acta Crystallogr., Sect. B: Struct. Crystallogr. Cryst. Chem. **29**, 96 (1973).
[8] M. J. S. Dewar and E. G. Zoebisch, THEOCHEM **180**, 1 (1998); M. J. S. Dewar, E. G. Zoebisch, E. F. Healy, and J. J. P. Stewart, J. Am. Chem. Soc. **107**, 3902 (1985).
[9] A. St-Amant, D. R. Salahub, Chem. Phys. Lett. **169**, 387 (1990); A. St-Amant, Ph.D. thesis, University of Montreal, 1991.
[10] A. D. Becke, Phys. Rev. A **38**, 3098 (1988).
[11] J. P. Perdew, Phys. Rev. B **33**, 8822 (1986).
[12] K. Endo, Y. Kaneda, M. Aida, and D. P. Chong, J. Phys. Chem. Solids **56**, 1131 (1995).
[13] P. Skytt, J.-H. Guo, N. Wassdahl, J. Nordgren, Y. Luo, and H. Agren, Phys. Rev. A **52**, 3572 (1995).
[14] F. Kh. Gel'mukhanov and H. Agren, Phys. Rev. A **49**, 4378 (1994).
[15] Y. Ma, N. Wassdahl, P. Skytt, J.-H. Guo, J. Nordgren, P. D. Johnson, J.-E. Rubensson, T. Boske, W. Eberhardt, and S. D. Kevan, Phys. Rev. Lett. **69**, 2598 (1992).
[16] P. Skytt, P. Glans, D. Mancini, J.-H. Guo, N. Wassdahl, J. Nordgren, Y. Ma, and P. D. Johnson, Phys. Rev. B **50**, 10 457 (1994).
[17] P. Glans, P. Skytt, K. Gunnelin, J.-H. Guo, and J. Nordgren, in X-ray and Inner-Shell Process (Hamburg, Germany, 1996), edited by R. L. Johnson, H. Schmidt Backing, and B. F. Sohntag, AIP Conf. Proc. No. **389** (AIP, Woodbury, NY, 1997), p. 723.
[18] P. Glans, K. Gunnelin, P. Skytt, J.-H. Guo, N. Wassdahl, J. Nordgren, H. Agren, F. Kh. Gelmukhanov, T. Warwick, and E. Rotenberg, Phys. Rev. Lett. **76**, 2448 (1996).
[19] P. Glans, P. Skytt, K. Gunnelin, J.-H. Guo, and J. Nordgren, J. Electron Spectrosc. Relat. Phenom. **82**, 193 (1996).
[20] J.-H. Guo, M. Magnuson, S. Sathe, J. Nordgren, L. Yang, Y. Luo, H. Agren, K. Z. Xing, N. Johansson, W. R. Salaneck, R. Daik, and W. J. Feast, J. Chem. Phys. **108**, 5990 (1998).